Phys. Med. Biol., 1990, Vol. 35, No 4, 501–516. Printed in the UK

Correction factors for thick-walled ionisation chambers in point-source photon beams

Alex F Bielajew

Division of Physics, Ionizing Radiation Standards, National Research Council of Canada, Ottawa, Canada K1A 0R6

Received 6 June 1989, in final form 16 November 1989

Abstract. In absolute exposure and air kerma measurements, such as those performed at Standards' laboratories, axial and radial non-uniformity correction factors are used to account for the non-uniformity of the incident photon field in the vicinity of the ionisation-chamber cavity. In this paper a theory for calculating the correction due to source non-uniformity is developed which applies to thick-walled ionisation chambers irradiated by point-source photon fields with arbitrary incident energy distributions. The equations are derived within the framework of a fundamental theory of ionisation-chamber response and are suitable for Monte Carlo calculation. Monte Carlo calculations for estimating the correction in pancake, cylindrical and spherical geometries are described and comparisons with the experimental results of Kondo and Randolph indicate agreement to better than 0.5% demonstrating the viability of the theory under even the most extreme measurement conditions.

1. Introduction

When a detector is placed in the field of a radiation source, the point at which the radiation field is being measured is uncertain, owing to the finite size of the detector. In the realm of exposure or air kerma measurement, one assumes that the 'point of measurement' is at the geometric centre of the chamber and the correction for the departure in ionisation-chamber response from the inverse-square law is accounted for by the 'axial' non-uniformity correction factor, k_{an} and in part, by the 'radial' non-uniformity correction factor, k_{rn}. The axial factor is a correction for the non-uniformity of the photon field along the line from the source through the cavity centre while the radial factor accounts for non-uniformity in the perpendicular direction arising not only from the point-source $1/r^2$-dependence but also from air, collimator and room scatter as well as finite source-size effects.

Since there are divergent views as to how such a correction is to be applied (Gray 1937b, Failla and Marinelli 1937, Mayneord and Roberts 1937, Spiers 1941, Burlin 1959, Kondo and Randolph 1960, Boutillon and Niatel 1973, Loftus and Weaver 1974, Shortt and Ross 1986), this question is addressed anew aided by Monte Carlo methods to serve as a calculational tool along with the employment of a consistent theoretical framework that describes thick-walled ionisation-chamber response (Bielajew 1986). In this paper the primary focus will be to demonstrate the viability of the new theory by applying it to measured data obtained under very stringent experimental conditions.

The application of the theory to small chambers at practical measurement distances is reserved for the companion paper (Bielajew 1990).

2. The theory

In a previous paper (Bielajew 1986) a fundamental theory of thick-walled ionisation-chamber response to photon beams was developed. This theory is fundamental in the sense that it is derived from first principles starting with a statement of the conservation of energy. Equations for perturbation factors were derived which quantified the departure of experimental conditions from those assumed in the Bragg–Gray theory (Bragg 1912, Gray 1929, 1936, 1937a,b) and in the Spencer–Attix (1955) theory of ionisation-chamber response due to scatter and attenuation of the primary photon beam. This theory of ionisation-chamber response (Bielajew 1986) was limited to uniform, monoenergetic incident photon fields although it was suggested how the theory could be modified to account for any incident energy distribution. The theory is now developed further to account for an arbitrary incident energy distribution and, in particular, for a point-source distribution of the incident primary photon beam. Although the discussion is restricted to a point-source distribution, the theory may easily be extended to other distributions.

2.1. Energy conservation for uniform beams in a uniform medium

The starting point is a statement of the conservation of energy. Consider a primary photon energy fluence, $\Psi^0(E_\gamma)$, in space (vacuum or air, no chamber present) which is spatially uniform. For the present, consider only monoenergetic photons with energy E_γ. Let the incident photon field impinge on a uniform medium which is large enough so that there exists some smaller region within it such that any electron which is set in motion directly by the incident photon field cannot escape through a boundary. In this smaller region a state of *quasi* charged particle equilibrium exists. The effect of attenuation of the primary photon fluence must be undone to produce a *true* charged particle equilibrium in the region. Energy conservation for the equilibrium region can be expressed as

$$\Psi^0(E_\gamma)(\mu_{\rm en}(E_\gamma)/\rho)_{\rm m} = \int \frac{{\rm d}\boldsymbol{r}'}{V} \int {\rm d}E_{\rm e} \exp(\Sigma_{\rm m}(E_\gamma)|\boldsymbol{r}' - \boldsymbol{r}_{\rm s}|)\Phi^0_{E_{\rm e}}(\boldsymbol{r}', |\boldsymbol{r} - \boldsymbol{r}'|, \theta_{\boldsymbol{r}',\boldsymbol{r}-\boldsymbol{r}'}, E_{\rm e}, E_\gamma)(S_{\rm col}(E_{\rm e})/\rho)_{\rm m} \tag{1}$$

which equates the energy *transferred* (less radiative losses) to electrons (left hand side) to the energy *deposited* by the electrons in collision processes (right hand side). In this equation, $(\mu_{\rm en}/\rho)_{\rm m}$ is the mass energy-absorption coefficient for the medium 'm' evaluated at the primary photon energy. The primary electron fluence, $\Phi^0_{E_{\rm e}}$, differential in the electron energy, $E_{\rm e}$, depends explicitly on $\boldsymbol{r}'$, the position of the initiating photon interaction (owing to the attenuation of the primary photon beam), on $|\boldsymbol{r} - \boldsymbol{r}'|$, the distance between the point of energy deposition and the initiating interaction point, on $\theta_{\boldsymbol{r}',\boldsymbol{r}-\boldsymbol{r}'}$, the angle of $\boldsymbol{r} - \boldsymbol{r}'$ with respect to the initiating photon's direction, and on $E_{\rm e}$ and E_γ. The integration, $\int {\rm d}\boldsymbol{r}'/V$, takes place over a volume large enough to contain all possible initial interaction points which can produce an electron fluence at $\boldsymbol{r}$. The factor $\exp(\Sigma_{\rm m}(E_\gamma)|\boldsymbol{r}' - \boldsymbol{r}_{\rm s}|)$ counterbalances the effect of primary photon attenuation

and renders the right hand side of (1) independent of $\boldsymbol{r}$ in the equilibrium region†. This factor was discussed previously (Bielajew 1986) although it is now expressed in a different form. The quantity Σ_m is the macroscopic primary photon interaction cross section and $|\boldsymbol{r}' - \boldsymbol{r}_s|$ is the distance the primary photon travelled beneath the surface of the medium having started at a point on the surface, $\boldsymbol{r}_s$ and having interacted at $\boldsymbol{r}'$. The unrestricted mass collision stopping power for the medium, $(S_{col}/\rho)_m$, evaluated at the electron energy, provides the means for the electrons to transfer energy to the medium. It is not germane to the derivation that no δ-rays were included and an unrestricted stopping power was used. Restricted stopping powers could have been used and δ-rays included at the expense of an even more cluttered notation. In fact, any electron energy deposition scheme may be used as long as the energy balance expressed by (1) is preserved. However, the evaluation of expressions will depend on what energy deposition scheme is employed.

2.2. Extension to a point source

The assumption that the incident photon fluence is spatially uniform may also be relaxed. Assume that it has a point-source dependence, $\Psi^0(E_\gamma, \boldsymbol{r}) = (r_0^2/r^2)\Psi^0(E_\gamma, \boldsymbol{r}_0)$, referring the primary photon energy fluence to some arbitrary point, $\boldsymbol{r}_0$. The vector $\boldsymbol{r}_0$ defines the point of measurement as this is the location at which the photon fluence is to be measured.

An arbitrary incident photon energy spectrum is now included as well. Then, suppressing most of the functional dependence, equation (1) for the energy deposition at $\boldsymbol{r}$ may be rewritten

$$\int dE_\gamma r_0^2 \Psi^0_{E_\gamma}(\boldsymbol{r}_0)(\mu_{en}/\rho)_m = \int dE_\gamma \int \frac{d\boldsymbol{r}'}{V} \int dE_e u(\boldsymbol{r}', \boldsymbol{r}) \tilde{\Phi}^0_{E_e, E_\gamma}(S_{col}/\rho)_m \tag{2}$$

where both the photon energy fluence and electron fluence are now differential in the incident photon energy and the definition $\tilde{\Phi}^0 = \Phi^0 \exp(\Sigma_m(E_\gamma)|\boldsymbol{r}' - \boldsymbol{r}_s|)$ is effected for brevity. The 'unweighting' function, $u(\boldsymbol{r}', \boldsymbol{r})$, completely undoes the effect of the spatial variation of the incident primary photon beam on the electron fluence measured at $\boldsymbol{r}$ arising from a photon interaction at $\boldsymbol{r}'$ (see figure 1). The form of this unweighting function is

$$u(\boldsymbol{r}', \boldsymbol{r}) = (r)^2[1 - (|\boldsymbol{r} - \boldsymbol{r}'|/r)^2 \sin^2 \theta_{\boldsymbol{r}, \boldsymbol{r}-\boldsymbol{r}'}]^{1/2} \tag{3}$$

and is derived in appendix 2. Note that the integrand on the left-hand side of (2) has been multiplied by the analagous primary photon unweighting factor, r_0^2.

Having undone the attenuation of the primary beam as well as the spatial non-uniformity of the source, the left hand and right hand sides of (2) are independent of the position $\boldsymbol{r}$ as long as $\boldsymbol{r}$ is in the equilibrium region, that is, far enough from the boundaries of the medium so that local energy conservation still applies.

2.3. Correction factors for cavity measurements

The dose deposited in the gas cavity of a thick-walled ionisation chamber exposed to photon beams can be written implicitly as

$$D_g = \int d\Phi_g (S_{col}/\rho)_g \tag{4}$$

† This 'unweighting' technique is equivalent to the regeneration of the primary photons at the point of interaction which would produce an interacting but unattenuated primary photon beam. A proof of this equivalence is presented in appendix 1.

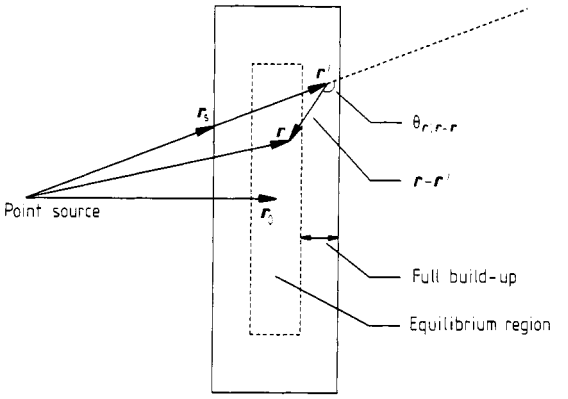

Figure 1. Definitions of the variables in (2). The full build-up walls delimit a region of electron equilibrium. Four vectors are defined: r_s, from the point source to surface of the chamber wall where the photon enters the chamber, r_0, from the point source to point of measurement (centre of the cavity for cavity chambers), r, from the point source to the point at which energy is being deposited by an electron, r', from the point source to the point of interaction where an incident photon interacts to produce an electron that deposits energy at r. The angle, $\theta_{r',r-r'}$ is the angle between r' and $r-r'$.

where the shorthand notation,

$$\int d\Phi_g \longrightarrow \int_g \frac{dr}{V_g} \int dE_\gamma \int_{ch} \frac{dr'}{V_{ch}} \int dE_e \Phi^g_{E_e,E_\gamma}$$

is used. The integral, $\int_g dr/V_g$, sums the electron energy deposition over all points in the gas cavity and the integral, $\int_{ch} dr'/V_{ch}$, sums all contributions to the electron fluence at r arising from all possible points where the electrons were set in motion in either the chamber walls or gas. The stopping power appropriate for the cavity gas, $(S_{col}/\rho)_g$, is used. In (4) the electron fluence, Φ_g, contains all electrons that may be present in the region of the cavity (δ-rays excluded) that may arise due to primary or scattered photons. The subscript or superscript 'g' on the electron fluence signifies that the electron fluence in the region of the cavity is to be calculated with gas as the cavity material.

Following the technique discussed in the earlier report (Bielajew 1986), the contribution of secondary scatter, the electrons which are set in motion by other than the primary photons, may be 'split off' and the effect of photon attenuation may be separated as well. Remaining factors may be identified as either a fluence perturbation owing to material difference between the wall and cavity or a geometric perturbation due to the non-uniformity of the incident photon field. The result is that the dose to the cavity gas may be expressed as

$$D_g = K_g(r_0)(\overline{\mu_{en}})^w_g(\bar{s})^g_w A_{sc} A_{at} A_{fl} A_{pn} \tag{5}$$

where the collision kerma to the gas at the point of measurement, $K_g(r_0)$, is

$$K_g(r_0) = \int dE_\gamma \Psi^0_{E_\gamma}(r_0)(\mu_{en}/\rho)_g \tag{6}$$

and the ratio of mass energy-absorption coefficients is defined to be

$$(\overline{\mu_{en}})^w_g = K_w/K_g. \tag{7}$$

The mass stopping-power ratio is defined to be

$$(\bar{s})^{g}_{w} = \left(\int d\tilde{\Phi}^{0}_{w} u(r', r)(S_{col}/\rho)_{g}\right)\left(\int d\tilde{\Phi}^{0}_{w} u(r', r)(S_{col}/\rho)_{w}\right)^{-1}. \tag{8}$$

The *primary photon scatter* correction factor, A_{sc}, can be written as

$$A_{sc} = 1 + \left(\int d(\Phi_{g} - \Phi^{0}_{g})(S_{col}/\rho)_{g}\right)\left(\int d\Phi^{0}_{g}(S_{col}/\rho)_{g}\right)^{-1} \tag{9}$$

where the primary electron fluence, Φ^{0}_{g}, is defined as the fluence of only those electrons that arise directly from the primary interaction of the incident photons. The *primary photon attenuation* correction factor, A_{at}, can be written as†

$$A_{at} = \left[1 + \left(\int d(\tilde{\Phi}^{0}_{g} - \Phi^{0}_{g})(S_{col}/\rho)_{g}\right)\left(\int d\Phi^{0}_{g}(S_{col}/\rho)_{g}\right)^{-1}\right]^{-1} \tag{10}$$

where $\tilde{\Phi}^{0}_{g} = \Phi^{0}_{g}\exp(\Sigma_{ch}(E_{\gamma})|r' - r_{s}|)$ is defined. The macroscopic cross section, Σ_{ch}, is written with a subscript 'ch' to denote that it should be computed for the entire chamber, walls and gas cavity included. One should note that both A_{at} and A_{sc} depend on the source-to-chamber distance since the primary photon pathlengths through the chamber change with distance. In most cases this dependence is weak.

The *fluence perturbation* correction factor, A_{fl}, is defined as

$$A_{fl} = \lim_{r_{0}\to\infty}\left[\left(\int d\tilde{\Phi}^{0}_{g} u(r', r)(S_{col}/\rho)_{g}\right)\left(\int d\tilde{\Phi}^{0}_{w} u(r', r)(S_{col}/\rho)_{g}\right)^{-1}\right] \tag{11}$$

and a new quantity, the *point-source non-uniformity correction factor* is defined to be

$$A_{pn} = \left[\left(r_{0}^{2}\int d\tilde{\Phi}^{0}_{g}(S_{col}/\rho)_{g}\right)\left(\int d\tilde{\Phi}^{0}_{w} u(r', r)(S_{col}/\rho)_{g}\right)^{-1}\right] A_{fl}^{-1}. \tag{12}$$

The subscript 'w' on the electron fluence in (8), (11) and (12) signifies that the electron fluence in the location of the cavity is to be calculated with wall material substituting the gas.

The unweighting factor undoes the effect of the spreading of the beam implying that $(\bar{s})^{g}_{w}$ expressed by (8) is independent of the chamber-cavity geometry and source-to-chamber distance. Using the limit

$$\lim_{|r-r'|,|r_{0}-r|\ll r_{0}} u(r', r) \longrightarrow r_{0}^{2} \tag{13}$$

and the realisation that the electron fluence per unit incident photon fluence in the large distance point-source limit is the same as that in a parallel photon beam, the stopping-power ratio expressed by (8) is identical to that calculated in a uniform, parallel beam. That is

$$(\bar{s})^{g}_{w} = \lim_{r_{0}\to\infty}\left[\left(\int d\tilde{\Phi}^{0}_{w}(S_{col}/\rho)_{g}\right)\left(\int d\tilde{\Phi}^{0}_{w}(S_{col}/\rho)_{w}\right)^{-1}\right] \tag{14}$$

† In a previous paper (Bielajew 1986) A_{at} was written βA^{0}_{att} to emphasise that electron drift downstream from the point of interaction was included in the primary attenuation correction factor.

recovering the parallel beam definition discussed previously (Bielajew 1986). Thus, $(\bar{s})^{g}_{w}$ may be calculated (or measured) in a parallel beam. This equivalence shall be demonstrated later by explicit calculation.

In the parallel beam limit (infinite source distance) the fluence perturbation factor, A_{fl}, measures the perturbation of the primary electron fluence in the chamber cavity due to the presence of a different medium in the cavity, corrected for photon attenuation. An expression equivalent to (11) is,

$$A_{fl} = \lim_{r_0 \to \infty} \left[\left(\int d\tilde{\Phi}^0_g (S_{col}/\rho)_g \right) \left(\int d\tilde{\Phi}^0_w (S_{col}/\rho)_g \right)^{-1} \right] \tag{15}$$

owing to the asymptotic behaviour of the unweighting factor and the electron fluences. Although this definition may seem arbitrary, it recovers the definition of the fluence perturbation as expressed previously for uniform beams (Bielajew 1986). A basic assumption of Bragg–Gray cavity theory is that this fluence perturbation is unity and this shall be assumed to be true for the present discussion. Again, this factor may equally well be calculated (or measured) in a parallel beam.

Finally, the remaining perturbation is collected in the factor A_{pn} and this correction is interpreted as the variation of the response owing to the spatial variation of the incident photon fluence. This correction factor depends explicitly on the point of measurement and can contain significant dependence on the source–chamber distance. The scatter and attenuation corrections can also contain some distance dependence, but the dominant behaviour is contained in A_{pn}. Using (11) and (13), A_{pn} may also be written

$$A_{pn} = \left(r_0^2 \int d\tilde{\Phi}^0_g (S_{col}/\rho)_g \right) \left(\lim_{r_0 \to \infty} r_0^2 \int d\tilde{\Phi}^0_g (S_{col}/\rho)_g \right)^{-1} \tag{16}$$

and the interpretation is evident as the ratio of the response per unit incident photon fluence (scatter and attenuation corrected) for a finite distance from the point source over the infinite distance limit, or equivalently, the parallel beam limit. This is more or less the expression one would write down intuitively for the field non-uniformity correction.

With the help of the unweighting factor expressed by (3), (8), (11) and (12) may be used interchangeably with (14)–(16). In fact, the form of the unweighting function is not needed to derive the final expressions in (14)–(16), merely proof of its existence. However, questions of existence are put aside by explicit characterisation of the unweighting function. Moreover, it may be more efficient computationally to calculate the stopping power and non-uniformity correction using (8) and (12) since the parallel beam calculation is not needed.

3. Applications

In this section Monte Carlo calculations of ionisation-chamber response and correction factors are described . The EGS4 code system (Nelson *et al* 1985) was employed with the PRESTA electron transport algorithm (Bielajew and Rogers 1987) that has been shown to calculate absolute ionisation-chamber response reliably for carbon-walled chambers. The PRESTA algorithm used in its default configuration is known to underestimate

electron backscatter, an effect that becomes more pronounced for high-Z materials. Therefore, in one case where a copper chamber was studied, an additional restriction on electron step-size was used whereby the maximum amount of energy loss to 'continuous' processes for each electron step-size was restricted to 1.0%. (ESTEPE was set to 0.01 (Rogers 1984).) The EGS4 user codes employed in this report, CAVRZ (cylindrical-planar geometry) and CAVSPH (spherical-conical geometry), are derivatives of CAVITY, which has been used previously to calculate scatter and attenuation correction factors (Bielajew *et al* 1985, Rogers *et al* 1985). The reliability of the Monte Carlo calculations is within the stated uncertainties, which were estimated by dividing the calculation into 10 batches and calculating the estimated variance of the mean. A minimum of about 7.5×10^5 incident photon interactions were used for each simulation although as many as 3×10^6 histories were used for some cases. Each photon was 'forced' to interact at least once in the chamber (a standard 'variance reduction' technique, see, for example Rogers and Bielajew (1984)). The simulations were performed on an IBM 3090 and typical simulation times were 1–8 CPU h per chamber for each distance.

The unweighting factor was not used in its exact form, rather the approximation $u(\boldsymbol{r}', \boldsymbol{r}) \approx (r)^2$ was used. As seen from the exact expression in (3), this approximation is valid to order $(r_e/r_0)^2$, where r_e is the electron range in the wall material. This approximation holds in the present context where the electron range is at most a few millimetres and the smallest source to chamber mid-point distance is of the order of a few centimetres.

To improve the efficiency of the Monte Carlo calculations, a correlated sampling technique was used to calculate A_{pn}. Referring to (12) which was used to calculate A_{pn}, some degree of correlation between the numerator and denominator (inside the square brackets) may be exploited. In the calculation of the numerator, if a primary photon passed through the cavity or a primary electron or one of its δ-rays deposited energy in the cavity, then this history was restarted with the same initial random number for the denominator where the cavity is filled with wall material. The numerator is essentially the primary dose to the cavity filled with gas. Thus, the primary dose and A_{pn} are correlated. Hence, A_{pn} can be calculated with more statistical accuracy than the primary dose, and the response corrected by A_{pn} can be more accurate then either the raw calculated response or A_{pn}.

3.1. Comparison with Kondo and Randolph

Kondo and Randolph (1960) measured ionisation-chamber response versus source-to-detector distance for large spherical and cylindrical chambers in low scatter conditions with a small ^{60}Co source, closely approximating a point source. For the latter chamber they oriented the chamber with the beam directed both on the side and on the end of the chamber. To account for departure from $1/r^2$ behaviour, they also proposed a 'surface' theory which agreed with experiment to within about $\pm 2\%$ for their sphere and $\pm 3\%$ for their cylinder. This paper is not intended to discuss their theory but makes use of their experimental results only. A minor difficulty in this comparison arises from their employment of chambers that did not have full build-up thickness walls. A direct comparison of the Monte Carlo results with experiment was performed although it caused $A_{pn}(\infty) \equiv \lim_{r_0 \to \infty} A_{pn}(r_0)$ to be significantly different from unity, as low as 0.9. The reason for this is evident from (12), where the denominator (inside the square brackets) is calculated with wall material in the cavity. When incomplete build-up walls are used, the substitution of the gas by wall material can cause most of the cavity region to have full build-up. Hence, the asymptotic value of $A_{pn}(\infty)$ is

expected to be less than unity in this case. The Monte Carlo calculations also ignored any possible electron contamination that could penetrate the thin walls. Electrons are set in motion both in the source capsule and in the air. The source capsule electrons scattered by the air away from the detector are, to first approximation, compensated for by a build-up of the air-generated electrons (Rogers *et al* 1988). Since these electrons should be emitted isotropically in a fashion similar to the primary photons, the effect of electron contamination should be minimal in a relative comparison.

One set of measurements employed a spherical copper chamber with 0.215 g cm^{-2} thick walls and a 4.82 cm internal radius. The source distances ranged from about 5.5 cm to 65 cm from the centre of the detector. The raw measured and calculated responses are shown in figure 2 as well as the Monte Carlo calculated responses corrected for scattering by A_{sc} (from (9)), for attenuation and electron drift by A_{at} (from (10)), and most importantly by A_{pn} from (12). Owing to the use of an incomplete build-up wall thickness $A_{pn}(\infty)$, as obtained by taking the limit of (12), was 0.897 ± 0.005. The stopping-power ratio, calculated from (8), did not vary by more than 0.0002 over all the distances.

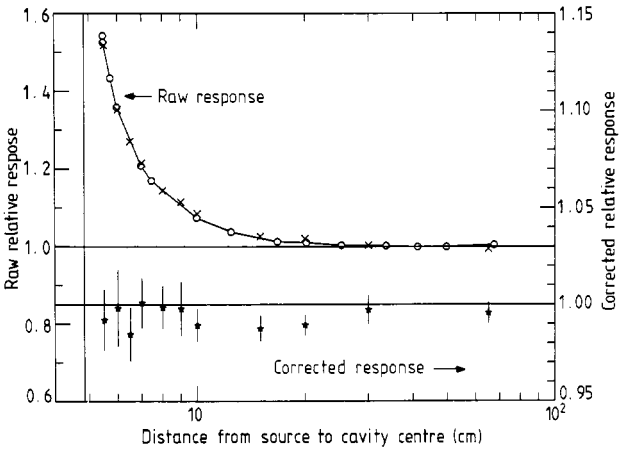

Figure 2. Raw and corrected responses of the spherical chamber relative to the parallel beam Monte Carlo calculation. Once corrected for point-source non-uniformity and wall perturbations, the chamber response shows no deviation with distance from the source to within the average 0.9% precision of the Monte Carlo calculation. Crosses, Monte Carlo; open circles, measurements. Cu sphere, 9.64 cm diameter.

The raw Monte Carlo responses are in excellent agreement with the experimental data. In this, and the subsequent comparisons with experimental data, the corrected and raw Monte Carlo data are normalised to the calculated corrected parallel beam results. The experimental data were normalised to the raw Monte Carlo responses by an 'eyeball' fit. The estimated precision of the raw Monte Carlo responses is about 0.5%. Once corrected, the Monte Carlo responses (or the experimental results if one had chosen to correct them instead) show no further distance dependence to within the estimated average 0.9% precision of the corrected Monte Carlo responses.

The correction factors, which provide more than 50% correction close to the source, are plotted in figure 3. The estimated average statistical uncertainty of the calculated correction factors is about 1.2% for $A_{pn}/A_{pn}(\infty)$ and about 0.1% for $A_{wall} \equiv A_{at} \times A_{sc}$. For this chamber there is only a small dependence of A_{wall} on distance ranging from about 0.981 at small distances to about 0.987 at large distances.

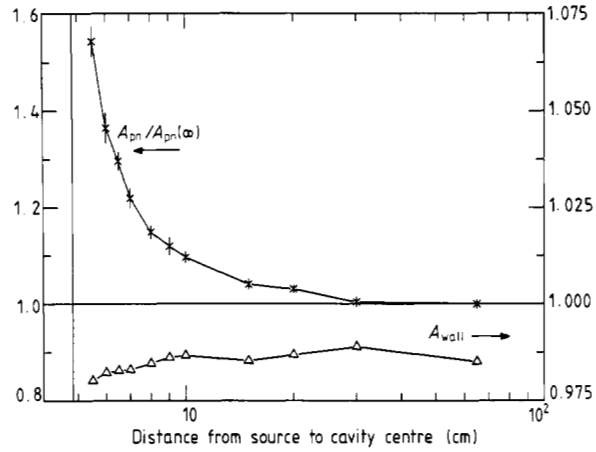

Figure 3. $A_{pn}/A_{pn}(\infty)(\times)$ and $A_{wall} \equiv A_{at} \times A_{sc}(\triangle)$ correction factors for the spherical chamber.

Another set of measurements employed a Victoreen 0.25R chamber (it was assumed to be model number 130), a cylindrical chamber with a 4.78 cm internal diameter, 10.53 cm inner depth, and a 0.212 g cm^{-2} wall composed of a 'phenolic' plastic. Despite repeated effort, the exact composition and density of this wall material were not obtainable from the manufacturer. In the simulations, the wall was assumed to have an equivalent thickness of Delrin (1.425 g cm^{-3}), which should have the same elemental composition as a phenolic plastic. In this set of measurements, the irradiation was from the side and the distances ranged from about 2.75 cm to about 31 cm from the centre of the detector. The raw measured and calculated responses are shown in figure 4 as well as the Monte Carlo calculated responses corrected by A_{sc}, A_{at} and A_{pn}.

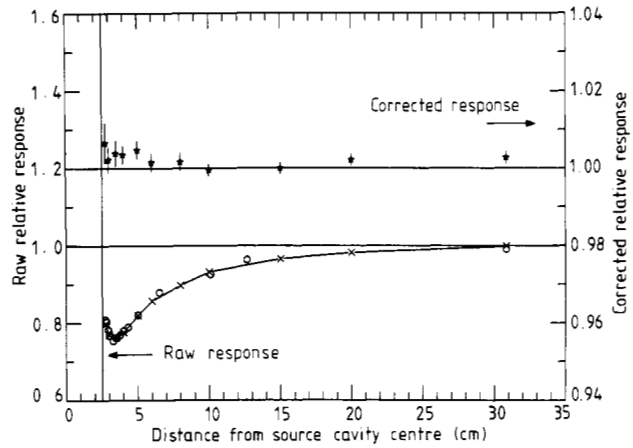

Figure 4. Raw and corrected responses of the cylindrical chamber with irradiation from the side relative to the parallel beam Monte Carlo calculation. Once corrected for point-source non-uniformity and wall perturbations, the chamber response shows no significant deviation with distance from the source to within the average 0.2% precision of the Monte Carlo calculation. Crosses, Monte Carlo; open circles, measurements. Plastic cylinder—beam on side, length 10.53 cm, diameter 5.78 cm.

Again, the raw Monte Carlo responses are in excellent agreement with the experimental data. The estimated precision of the raw calculated response is about 0.5%. After correction, the Monte Carlo results show no further distance dependence to within the estimated average 0.2% precision of the corrected Monte Carlo responses. In this case, because of the thin walls, $A_{pn}(\infty)$ attained a value of 0.916 ± 0.005. The stopping-power ratios did not vary by more than 0.0001 over the set of calculations.

The correction factors, which combine to provide up to a 27% correction close to the source, are plotted in figure 5. The estimated average statistical uncertainty of the calculated correction factors is about 0.5% for $A_{pn}/A_{pn}(\infty)$, and 0.1% for $A_{wall} = A_{at} \times A_{sc}$. For this chamber with the irradiation from the side, there is a more pronounced dependence of A_{wall} on distance ranging from about 0.983 at small distances to about 0.996 at the large distances.

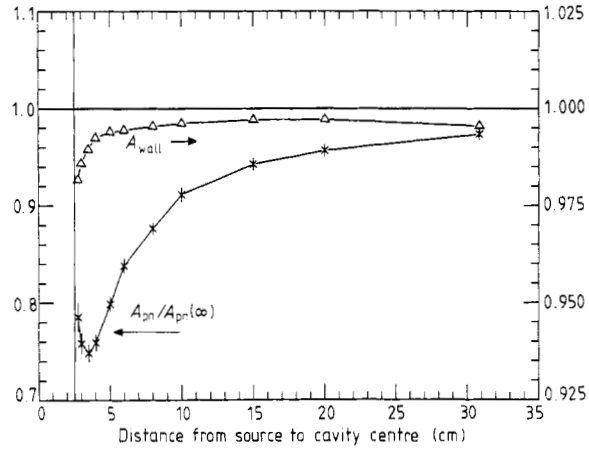

Figure 5. $A_{pn}/A_{pn}(\infty)(\times)$, and $A_{wall} = A_{at} \times A_{sc}(\triangle)$ correction factors for the cylindrical chamber irradiated from the side.

Finally, the same cylindrical chamber was employed with the irradiation from the front with the distances ranging from about 6.8 cm to about 66 cm from the centre of the detector. As seen in figure 6, the raw Monte Carlo responses are again in excellent agreement with the experimental data. The estimated precision of the raw Monte Carlo responses is about 0.4%. After correction, the Monte Carlo results show a distance dependence of about 0.5%. The estimated average precision of the corrected Monte Carlo responses is about 0.4%. In this case, because of the thin walls, $A_{pn}(\infty)$ attained a value of 0.955 ± 0.006. Any distance dependence in this case can probably be ascribed to the employment of thin walls for the chamber. The stopping-power ratios did not vary by more than 0.0001 over the set of calculations.

The correction factors, which combine to provide more than 100% correction close to the source, are plotted in figure 7. The estimated average statistical uncertainty of the calculated correction factors is about 0.5% for $A_{pn}/A_{pn}(\infty)$, and 0.06% for $A_{wall} = A_{at} \times A_{sc}$. For this chamber with the irradiation from the front, there is significant dependence of A_{wall} on distance ranging from about 1.003 at small distances to about 0.958 at the largest distance measured.

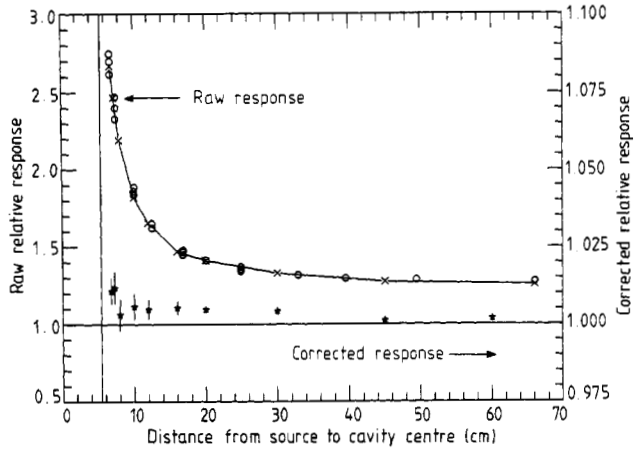

Figure 6. Raw and corrected responses of the cylindrical chamber with irradiation from the front relative to the parallel beam Monte Carlo calculation. Once corrected for point-source non-uniformity and wall perturbations, the chamber response shows a small ($\approx$ 0.5%) deviation with distance. The precision of the Monte Carlo calculation is about 0.4%. Crosses, Monte Carlo; open circles, measurements. Plastic cylinder—beam on front, length 10.53 cm, diameter 5.78 cm.

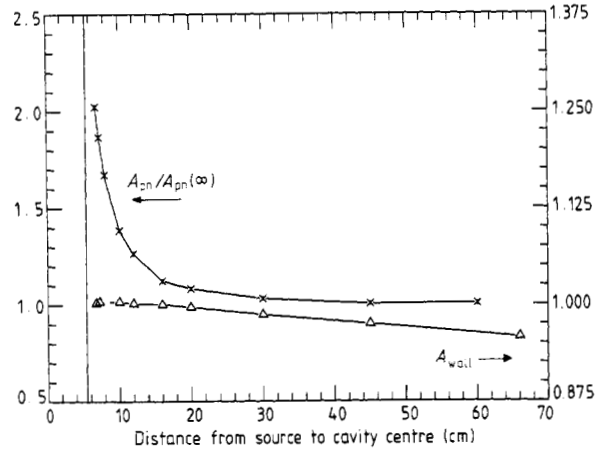

Figure 7. $A_{pn}/A_{pn}(\infty)(\times)$, and $A_{wall} = A_{at} \times A_{sc}(\triangle)$ correction factors for the cylindrical chamber irradiated from the front.

4. Conclusions

The formal theory expressed in (5)–(12), and (14)–(16) corrects for departures from $1/r^2$ behaviour for even the most extreme source-to-chamber distances providing corrections as large as a factor of 2 in some of the cases studied. In the worst case studied, the corrections account for deviations to within 0.5% although even this disagreement can probably be ascribed to the use of thin walls in the experiment. The theory relies upon the existence of a point-source unweighting factor that undoes the effect of beam spreading in a uniform medium. This factor is derived rigorously in appendix 2. A simple approximation to the correction factor in the form of r^2 was employed that breaks down only when the source-to-chamber distance is comparable to the electron

range in the chamber walls.

A new correction factor, A_{pn}, is proposed to correct both for axial non-uniformity and the portion of radial non-uniformity associated with the non-uniformity of the field in the radial direction due to $1/r^2$ fall-off. Other radial non-uniformities associated with collimator, air and room scatter and finite source-size effects are not considered. A possible way to account theoretically for these effects may be effected by considering an extended source, each element of which is a point source, and integrating over these point-source elements in (2) and subsequent expressions. Alternatively, one may obtain the suitable unweighting factor in a similar fashion to that employed in appendix 2.

Theoretical forms for the other familiar correction factors were described as well. The attenuation correction, A_{at}, and scatter correction, A_{sc}, both depend on the source-to-chamber distance, albeit weakly. The stopping-power ratio and fluence correction, A_{fl}, are both given as parallel beam ($r_0 \longrightarrow \infty$) quantites. The unweighting factor also allows the parallel beam value to be attained at any source-to-chamber distance. The stability of the stopping-power ratio given in the examples corroborates the equivalent forms given in (8) and (14) and lends indirect credence to the unweighting factor.

It remains to employ this theory for more practical measurements—chambers a few centimetres across at most, not closer than 1 m from the source. Unfortunately, to be of practical use A_{pn} should be calculated to better than 0.1% statistical accuracy requiring hundreds of hours of CPU time on even the fastest computers available. To preview the companion paper (Bielajew 1990), an analytic theory is developed to help in the extrapolation to large distances where the corrections may be small but, nonetheless, of great importance, especially for absolute measurements performed in Standards' laboratories.

Acknowledgments

The author wishes to express his appreciation to his colleagues Dr David W O Rogers and Dr Carl K Ross for numerous enlightening and spirited discussions.

Appendix 1. Equivalence of photon attenuation unweighting and regeneration

Consider the following equation as a mathematical model of primary dose deposition

$$D^0(\lambda) = \int_0^\Lambda d\lambda_1 \exp(-\lambda_1) f^0(\lambda - \lambda_1), \tag{A1.1}$$

where the distance beneath the surface of the chamber is measured in mean free paths, λ, and the total thickness of the chamber in the direction of the incident photon at the point the photon enters the chamber is Λ. The exponential attenuation is made explicit, and the dose deposition about the point of interaction, λ_1, is expressed by f^0. All other direction dependencies do not depend on λ and may be integrated out.

Consider the unweighting method with the attenuation unweighting factor $\exp(\lambda_1)$ in the integrand

$$D_u^0(\lambda) = \int_0^\Lambda d\lambda_1 \exp(-\lambda_1) \exp(\lambda_1) f^0(\lambda - \lambda_1) = \int_0^\Lambda d\lambda_1 f^0(\lambda - \lambda_1). \tag{A1.2}$$

This is the method by which the attenuation correction is calculated by the Monte Carlo simulations since it allows efficient computation because the weighted and unweighted integrals are highly correlated.

Now consider the regenerative method whereby a photon, if it interacts, is regenerated. This results in an infinite series of integrals because, in principle, the photon can interact in the chamber any number of times. In our notation, the series takes the form

$$D_{\mathrm{r}}^{0}(\lambda) = \int_{0}^{\Lambda} \mathrm{d}\lambda_1 \exp(-\lambda_1)\{f^{0}(\lambda-\lambda_1) + \int_{\lambda_1}^{\Lambda} \mathrm{d}\lambda_2 \exp(\lambda_1-\lambda_2)\{f^{0}(\lambda-\lambda_2) + \int_{\lambda_2}^{\Lambda} \mathrm{d}\lambda_3 \exp(\lambda_2-\lambda_3)\{f^{0}(\lambda-\lambda_3)+\ldots. \tag{A1.3}$$

The nth-order term may be written

$$D_{\mathrm{r},n}^{0}(\lambda) = \int_{0}^{\Lambda} \mathrm{d}\lambda_1 \int_{\lambda_1}^{\Lambda} \mathrm{d}\lambda_2 \int_{\lambda_2}^{\Lambda} \mathrm{d}\lambda_3 \ldots \int_{\lambda_n}^{\Lambda} \mathrm{d}\lambda_{n+1} \exp(-\lambda_{n+1}) f^{0}(\lambda-\lambda_{n+1}). \tag{A1.4}$$

The orders of integration may be successively exchanged in the above integral (f^0 is assumed to be convergent enough to allow this) and the innermost integrals performed producing

$$D_{\mathrm{r},n}^{0}(\lambda) = \int_{0}^{\Lambda} \mathrm{d}\lambda_1 (\lambda_1^{n}/n!) \exp(-\lambda_1) f^{0}(\lambda-\lambda_1). \tag{A1.5}$$

Summing the series gives

$$D_{\mathrm{r}}^{0}(\lambda) = \int_{0}^{\Lambda} \mathrm{d}\lambda_1 \sum_{n=0}^{\infty} (\lambda_1^{n}/n!) \exp(-\lambda_1) f^{0}(\lambda-\lambda_1) = D_{\mathrm{u}}^{0}(\lambda) \tag{A1.6}$$

since $\sum_{n=0}^{\infty}(x^n/n!) = e^x$ for $x < 1$ and Λ is usually much less than unity for most practical chambers.

Thus, the unweighting method is equivalent to the regeneration method. The latter is far less efficient for practical chambers, however, as additional photons would have to be tracked through the chamber and one would lose much of the correlation in the ratio of weighted and unweighted integrals. The proof can probably be extended to arbitrary Λ owing to the localised behaviour of f^0. However, a more general proof will not be attempted since the above should suffice for most chambers. Note, however, that for extremely large chambers the unweighting factors may become very large, adversely affecting the calculation efficiency. In this case it may be preferable to switch to the regenerative technique.

Appendix 2. Derivation of the point-source unweighting factor

Consider the following expression for the equilibrium dose to a uniform medium in a non-attenuating, non-scattering parallel photon beam aligned with the z-axis

$$\tilde{D}^{0}(\boldsymbol{r}) = \int \mathrm{d}\boldsymbol{r}' \tilde{f}^{0}(|\boldsymbol{r}-\boldsymbol{r}'|, \cos\theta_{\hat{\boldsymbol{n}},\boldsymbol{r}-\boldsymbol{r}'}) \tag{A2.1}$$

where the integral occurs over a volume large enough to contain any electron that may drift to $\boldsymbol{r}$ having been set in motion at $\boldsymbol{r}'$, and $\tilde{f}^0$ is the equilibrium electron dose-deposition function that depends both on $|\boldsymbol{r}-\boldsymbol{r}'|$ and $\cos\theta_{\hat{\boldsymbol{n}},\boldsymbol{r}-\boldsymbol{r}'}$, the angle between $|\boldsymbol{r}-\boldsymbol{r}'|$ and the incident photon direction (unit vector $\hat{\boldsymbol{n}}$) which is fixed. The vectors $\boldsymbol{r}$ and $\boldsymbol{r}'$ are measured relative to any origin. Changing variables so that the integration occurs in the vicinity of the dose deposition, $\boldsymbol{r}''=\boldsymbol{r}-\boldsymbol{r}'$, gives the expression

$$\tilde{D}^0 = \int \mathrm{d}\boldsymbol{r}''\tilde{f}^0(|\boldsymbol{r}''|,\cos\theta_{\hat{\boldsymbol{n}},\boldsymbol{r}''}). \tag{A2.2}$$

Finally, the integration variable, $\boldsymbol{r}''$ may be rotated so that the angular integration variable is collinear with $\hat{\boldsymbol{n}}$ giving,

$$\tilde{D}^0 = \int \mathrm{d}\boldsymbol{r}''\tilde{f}^0(r'',\cos\theta'') \tag{A2.3}$$

where $r''=|\boldsymbol{r}''|$ and $\mathrm{d}\boldsymbol{r}''=(r'')^2\sin\theta''\mathrm{d}r''\mathrm{d}\theta''\mathrm{d}\phi''$. One sees explicitly that $\tilde{D}^0$ is a constant, independent of position.

For a point source, the point-source unweighted dose deposition equation becomes

$$\tilde{D}^0_{\mathrm{ps}}(\boldsymbol{r}) = \int \mathrm{d}\boldsymbol{r}'[u(\boldsymbol{r}',\boldsymbol{r})/|\boldsymbol{r}'|^2]\tilde{f}^0(|\boldsymbol{r}-\boldsymbol{r}'|,\cos\theta_{\boldsymbol{r}',\boldsymbol{r}-\boldsymbol{r}'}) \tag{A2.4}$$

where $u(\boldsymbol{r}',\boldsymbol{r})$ is the point-source unweighting function and $\cos\theta_{\boldsymbol{r}',\boldsymbol{r}-\boldsymbol{r}'}=[\boldsymbol{r}'\cdot(\boldsymbol{r}-\boldsymbol{r}')]/[|\boldsymbol{r}'||\boldsymbol{r}-\boldsymbol{r}'|]$ is the angle of the vector from the point of interaction to the point of energy deposition with respect to the incident photon direction which is now no longer fixed. The origin is situated at the location of the point source (see figure 1). Again, changing variables $\boldsymbol{r}''=\boldsymbol{r}-\boldsymbol{r}'$ to integrate over the region local to the dose deposition yields,

$$\tilde{D}^0_{\mathrm{ps}}(\boldsymbol{r}) = \int \mathrm{d}\boldsymbol{r}''[u(\boldsymbol{r}-\boldsymbol{r}'',\boldsymbol{r})/|\boldsymbol{r}-\boldsymbol{r}''|^2]\tilde{f}^0(r'',\cos\theta_{\boldsymbol{r}'',\boldsymbol{r}-\boldsymbol{r}''}). \tag{A2.5}$$

The second argument of the dose deposition function has the form

$$\cos\theta_{\boldsymbol{r}'',\boldsymbol{r}-\boldsymbol{r}''} = [\cos\theta_{\boldsymbol{r},\boldsymbol{r}''}-(r''/r)]\left[1-2(r''/r)\cos\theta_{\boldsymbol{r},\boldsymbol{r}''}+(r''/r)^2\right]^{-1/2} \tag{A2.6}$$

where $\cos\theta_{\boldsymbol{r},\boldsymbol{r}''}$ is the angle between $\boldsymbol{r}$ and $\boldsymbol{r}''$. Although this expression may seem complicated, $\cos\theta_{\boldsymbol{r}'',\boldsymbol{r}-\boldsymbol{r}''}$ may be used directly as the angular integration variable. In effect, one may rotate coordinates locally and measure angles relative to the incident photon direction. The resulting transformation yields

$$\tilde{D}^0_{\mathrm{ps}}(\boldsymbol{r}) = \int \mathrm{d}\boldsymbol{r}''u(\boldsymbol{r}-\boldsymbol{r}'',\boldsymbol{r})r^{-2}\left[1-(r''/r)^2\sin^2\theta_{\boldsymbol{r}'',\boldsymbol{r}-\boldsymbol{r}''}\right]^{-1/2}\tilde{f}^0(r'',\cos\theta''), \tag{A2.7}$$

where again, $\mathrm{d}\boldsymbol{r}''=(r'')^2\sin\theta''\mathrm{d}r''\mathrm{d}\theta''\mathrm{d}\phi''$. The mathematics involved in getting from (A2.5) to (A2.7) is straightforward but lengthy with substitution of variables and much cancellation. One may transform back putting the origin at the location of the point source and identify the unweighting factor

$$u(\boldsymbol{r}',\boldsymbol{r}) = (r)^2[1-(|\boldsymbol{r}-\boldsymbol{r}'|/r)^2\sin^2\theta_{\boldsymbol{r},\boldsymbol{r}-\boldsymbol{r}'}]^{1/2}. \tag{A2.8}$$

Thus identified, (A2.7) becomes

$$\tilde{D}^0_{ps}(\boldsymbol{r}) = \int d\boldsymbol{r}'' \tilde{f}^0(r'', \cos\theta'') \tag{A2.9}$$

identical to the expression given in (A2.3). Thus, $\tilde{D}^0_{ps}(\boldsymbol{r}) = \tilde{D}^0$, and is independent of location where the energy deposition is measured.

Résumé

Facteurs de correction pour des chambres d'ionisation à paroi épaisse utilisées dans des faisceaux de photons issus d'une source ponctuelle.

Lors de la détermination absolue de l'exposition et du kerma dans l'air, telle qu'elle est pratiquée dans les laboratoires d'étalonnage, on utilise des facteurs de correction axiale et radiale pour tenir compte du défaut d'uniformité du champ de photons incidents au voisinage de la cavité de la chambre d'ionisation. Dans ce travail, les auteurs développent une théorie permettant de calculer la correction de non uniformité due à la source, s'appliquant aux chambres d'ionisation à paroi épaisse irradiées par des faisceaux de photons issus de sources ponctuelles, avec des distributions d'énergies de photons incidents arbitraires. Les équations sont établies dans le cadre d'une théorie fondamentale de la réponse d'une chambre d'ionisation, et sont utilisables pour des calculs par la méthode de Monte Carlo. Les auteurs présentent les calculs effectués à l'aide de la méthode de Monte Carlo pour estimer la correction relative à des géométries planes, cylindriques et sphériques. Les comparaisons aux résultats expérimentaux de Kondo et Randolph mettent en évidence un accord meilleur qu'à 0.5% prés, démontrant la validité de la théorie, même dans les conditions de mesure les plus extrémes.

Zusammenfassung

Korrektionsfaktoren für dickwandige Ionisationskammern in Punktquellenphotonenstrahlen.

Bei Absolutmessungen der Ionendosis und der Kerma in Luft, so wie sie in Standardlaboratorien durchgeführt werden, werden axiale und radiale Inhomogenitätskorrecktionsfaktoren verwendet, um die Non-Uniformität des einfallenden Photonenfeldes in der Nähe von Ionisationskammerhohlräumen zu berücksichtigen. In der vorliegenden Arbeit wird eine Theorie entwickelt zur Berechnung der Korrektion aufgrund der Quellen-inhomogenität, anwendbar für dickwandige Ionisationskammern, die mit einem Punktquellenphotonenfeld mit willkürlicher Energieverteilung bestrahlt werden. Die Gleichungen wurden entwickelt im Rahmen einer grundlegenden Theorie des Ionisationskammerverhaltens und sind für Monte Carlo-Rechnungen geeignet. Monte Carlo-Rechnungen zur Bestimmung der Korrektion bei Flachkammern und Kammern mit Zylinder- und Kugelgeometrie werden beschrieben. Vergleiche mit den experimentellen Ergebnissen von Kondo und Randolph zeigen eine Ubereinstimmung besser als 0.5%, was die Bedeutung der Theorie auch unter extremen Meßbedingungen zeigt.

References

Bielajew A F 1986 Ionization cavity theory—a formal derivation of perturbation factors for thick-walled ion chambers in photon beams *Phys. Med. Biol.* **30** 161–70

—— 1990 An analytic theory of the point-source non-uniformity correction factor for thick-walled ionisation chambers in photon beams *Phys. Med. Biol.* **35** 517–538

Bielajew A F and Rogers D W O 1987 PRESTA—the parameter reduced electron-step transport algorithm for electron Monte Carlo transport *Nucl. Instrum. Methods* **B18** 165–81

Bielajew A F, Rogers D W O and Nahum A E 1985 The Monte Carlo simulation of ion chamber response to ^{60}Co—resolution of anomalies associated with interfaces *Phys. Med. Biol.* **30** 419–27

Boutillon M and Niatel M-T 1973 A study of a graphite chamber for absolute exposure measurements of ^{60}Co gamma rays *Metrologia* **9** 139–46

Bragg W H 1912 *Studies in Radioactivity* (London: Macmillan)

Burlin T E 1959 The measurement of exposure dose for high energy radiation with cavity ionization chambers *Phys. Med. Biol.* **3** 197–206

Failla G and Marinelli L D 1937 The measurement of the ionization produced in air by gamma rays *Am. J. Roentgenol.* **38** 312–43

Gray L H 1929 The absorption of penetrating radiation *Proc. R. Soc.* **A122** 647–68

—— 1936 An ionization method for the absolute measurement of γ-ray energy *Proc. R. Soc.* **A156** 578–96

—— 1937a Radiation dosimetry, Part I *Br. J. Radiol.* **10** 600–12

—— 1937b Radiation dosimetry, Part II *Br. J. Radiol.* **10** 721–42

Kondo S and Randolph M L 1960 Effect finite size ionization chambers on measurements small photon sources *Rad. Res.* **13** 37–60

Loftus T P and Weaver J T 1974 Standardization ^{60}Co and ^{137}Cs gamma-ray beams in terms exposure *J. Res. Nat. Bureau of Standards* **78A** 465–76

Mayneord W V and Roberts J E 1937 An attempt at precision measurements gamma rays *Br. J. Radiol.* **10** 365–88

Nelson W R, Hirayama H and Rogers D W O 1985 *The EGS4 Code System* Stanford Linear Accelerator Report SLAC-265 (Stanford, CA: SLAC)

Rogers D W O 1984 Low energy electron transport with EGS *Nucl. Instrum. Methods* **A227** 535–48

Rogers D W O and Bielajew A F 1984 *The Use of EGS for Monte Carlo Calculations in Medical Physics* NRCC Report PXNR-2692 (Ottawa: NRCC)

Rogers D W O, Bielajew A F and Nahum A E 1985 Ion chamber response and A_{wall} correction factors in a ^{60}Co beam by Monte Carlo simulation *Phys. Med. Biol.* **30** 429–43

Rogers D W O, Ewart G M, Bielajew A F and Van Dyk G 1988 Calculation electron contamination in a ^{60}Co therapy beam *Proc. IAEA Int. Symp. on Dosimetry in Radiotherapy* vol 2 (Vienna: IAEA) pp 303–12

Shortt K R and Ross C K 1986 *The Canadian ^{60}Co Exposure Standard* NRCC Report PIRS-0052 (Ottawa: NRCC)

Spencer L V and Attix F H 1955 A theory cavity ionization *Rad. Res.* **3** 239–54

Spiers F W 1941 Inverse square law errors in gamma-ray dose measurements *Br. J. Radiol.* **14** 147–56